80

Effects of Brain Ventricular Shape on Periventricular Biomechanics: A Finite-element Analysis

Alonso Peña, Ph.D., Malcolm D. Bolton, Ph.D.,
Helen Whitehouse, B.Sc.,
John D. Pickard, F.R.C.S., M.Chir., F.Med.Sci.

Academic Neurosurgery Unit (AP, HW, JDP) and Wolfson Brain Imaging Centre (AP, JDP), Addenbrooke's Hospital, and Department of Engineering (AP, MDB), University of Cambridge, Cambridge, England

OBJECTIVE: A computer simulation based on the finite-element method was used to study the biomechanics of acute obstructive hydrocephalus and, in particular, to define why periventricular edema is most prominent in the anterior and posterior horns.

METHODS: Brain parenchyma was modeled as a two-phase material composed of a porous elastic matrix saturated by interstitial fluid. The effects of the cerebrovascular system were not included in this model. The change in the shape of the ventricles as they enlarged was described by two variables, i.e., the stretch of the ependyma and the concavity of the ventricular wall. The distribution of stresses and strains in the tissue was defined by two standard mechanical measures, i.e., the mean effective stress and the void ratio.

RESULTS: With obstruction to cerebrospinal fluid flow, the simulation revealed that the degree of ventricular expansion at equilibrium depended on the pressure gradient between the ventricles and the subarachnoid space. Periventricular edema was associated with the appearance of expansive (tensile) stresses in the tissues surrounding the frontal and occipital horns. In contrast, the concave shape in the region of the body of the ventricle created compressive stresses in the parenchyma. Both of these stresses seem to be direct consequences of the concave/convex geometry of the ventricular wall, which serves to selectively focus the forces (perpendicular to the ependyma) produced by the increased intraventricular fluid pressure in the periventricular tissues.

CONCLUSION: The distribution of periventricular edema in acute hydrocephalus is a result not only of increased intraventricular pressure but also of ventricular geometry. (Neurosurgery 45:107–118, 1999)

Key words: Biomechanics, Finite-element analysis, Hydrocephalus, Periventricular edema

The acute stages of obstructive hydrocephalus are characterized by two main features, i.e., ventricular expansion and periventricular lucency (PVL), both of which can be clearly seen in computed tomographic and magnetic resonance imaging scans (1, 37, 49). Initially concentrated around the ventricular horns, PVL in the brain of younger patients is generally considered to represent a true increase in the extracellular spaces of tissue (3, 9, 22, 27, 36, 38, 39, 45, 46, 53). However, the biomechanical factors that condition its development are poorly understood (2, 40). PVL in the brain of aging patients has more complex causes, including ischemia, gliosis, and demyelination, as well as true edema.

It has been hypothesized that PVL may be attributable to 1) the intrusion of cerebrospinal fluid (CSF) into the white matter as a result of mechanical disruption of the ependyma (44), 2) periventricular stress concentrations (42), and/or 3) the geometry of the ventricular wall (51). The recent advances in our knowledge of the physical properties of brain tissue (24) and in finite-element computational methods (56) suggest that a quantitative investigation of these factors is timely and may shed light on how these factors interact with each other and on their possible roles in the sequence of events that lead to PVL.

In this study, therefore, we have proposed a set of definitions to evaluate quantitatively these three hypotheses, based on standard theories from the fields of continuum mechanics (19) and analytical geometry (52). These definitions have been used in conjunction with a two-dimensional, finite-element simulation of obstructive hydrocephalus (42, 43, 47, 51), in which brain parenchyma is modeled as a biphasic poroelastic material. Also, for the first time, an assessment of the accuracy

of the finite-element approximation involved has been performed (57).

MATERIALS AND METHODS

Brain tissue as a biphasic material

Hakim et al. (25, 26), the first authors to use the methods of continuum mechanics in the study of hydrocephalus, proposed that brain parenchyma can be regarded as "an open cell sponge made of viscoelastic material." Nagashima et al. (42, 43) formalized this concept in terms of the theory of poroelasticity (4) and the finite-element method (57). Since then, the view of brain tissue as a poroelastic material has been used in a number of studies (G Tenti, S Sivaloganathan, JM Drake, personal communication) (31, 47, 51).

In the present study, following the method of Hakim et al. (25, 26) and Nagashima et al. (42), brain parenchyma has been modeled as a linear poroelastic material composed of an elastic porous matrix saturated by an interstitial fluid in the pores. In this model, the volume occupied by the solids corresponds to the neurons and neuroglia, whereas the voids correspond to the extracellular space of the tissue. The effects of the cerebrovascular system are not included in this model.

The use of a biphasic poroelastic model for brain parenchyma is particularly appropriate because it allows direct computation of the transient changes in the regional solid/water contents of tissue (such as in edema) as a function of the sustained deformation. This capability is not available in other mechanical models that are monophasic, such as elastic, viscoelastic, and hyperelastic models (19).

The general theory for the mechanics of porous continua was initiated and formalized by Biot (4, 5). Other forms of this theory have been presented as the theory of mixtures (7); when applied to model the biomechanical behavior of soft tissues, they are equivalent (50). (For a comprehensive treatment, see the report by Coussy [13].) The linear theory of poroelasticity is based on the following principles: 1) linear elasticity of the solid matrix, 2) conservation of mass of the solid and fluid phases, 3) Darcy's law governing the diffusion of fluid through the pores of tissue, 4) equilibrium of forces, and 5) Terzaghi's principle of effective stress (see Appendix A).

Finite-element analysis

The differential equations, presented in Appendix A, represent what is termed in mathematics an initial-boundary value problem (IBVP). This represents the spatial and temporal relationships that the field variables ought to satisfy at every point in the domain of interest. The solutions of the IBVP are functions representing the history of the variables u and p. Simple boundary conditions and domains with simple geometries produce an IBVP that is amenable to producing exact or analytical solutions. However, this is seldom the case in applied mechanics, where complex geometries, boundary and initial conditions, and loads make the solution of the IBVP by exact mathematical methods practically impossible. In such cases, an approximate or numerical solution should be determined by the application of numerical analysis techniques based on computers. The finite-element method is a powerful example of such methods (57). Its advantages are its abilities to manage complex geometric domains, heterogeneities, load histories, and boundary conditions. In this study, we use the implementation of the finite-element method in the computer program ABAQUS/Standard (28), which was recently favorably benchmarked for the study of poroelastic materials (56).

The anatomic information needed to construct the finite-element mesh for our simulation was obtained from T2-weighted axial magnetic resonance imaging scans for a normal patient from the internet facility Whole Brain Atlas (30). Only one-half of the slice was used, given the symmetry of the brain in that section. One hundred sixty-seven points were digitally obtained and joined by straight lines to create the domain. From this domain, we generated our finite-element mesh using an automatic mesh-generating algorithm (14), which discretized the domain into 679 eight-noded quadrilateral elements, which are appropriate for consolidation analyses (*Fig. 1*).

The specific material properties of gray and white matter are controversial. In this study we assume the following experimental values, based on the most recent literature (24): $E = 10$ kPa, $v = 0.30$, $K = 10^{-11}$ $m^4N^{-1}s^{-1}$ (see discussion in Appendix B).

Two sets of boundary conditions, i.e., one for the solid phase and another for the fluid phase, are required for a consolidation analysis. The solid phase (the parenchyma) is assumed to be attached to the subarachnoid space and thus to be restricted to anterior-posterior movement along the midline and to be fixed at the end of the falx cerebri. The fluid pressure is assumed to be zero at the beginning of the analysis. A pressure gradient of 3.0 kPa (22.5 mm Hg) was established between the ventricular and subarachnoid spaces in the course of $t = 30{,}000$ seconds (8 h) simulated time. The initial conditions are zero displacements at the beginning of the analysis for the solid phase and 0 mm Hg of pressure for the fluid phase.

Measures of stress and strain

To be able to characterize the stress concentrations in the parenchyma, we propose to use the mean effective stress p' and the void ratio e, which are invariant measures of the effective stress and strain tensors of tissue (16, 19). Changes in geometry of the ventricles are captured by the stretch L of the

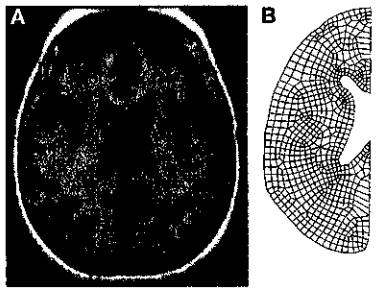

FIGURE 1. Axial magnetic resonance imaging scan for a normal subject (*A*) and the finite-element mesh used for the simulation (*B*). The mesh consisted of 679 quadrilateral elements and 2208 nodes. Only one-half of the scan was discretized, given the symmetry of the brain in this region.

ventricular wall and its concavity C. See *Figure 2* for explanatory diagrams and Appendix A for definitions.

The mean effective stress p'

$$p' = -\frac{1}{3}\,\mathrm{trace}(\sigma'_{ij}) \tag{1}$$

represents the average volumetric stress in a point of the parenchyma. This stress is the one uniquely responsible for the change in tissue volume.

The void ratio e

$$e = \frac{V^f}{V^s} \tag{2}$$

represents the volume of voids V^f (extracellular space) divided by the volume of solids V^s (cellular space) in a unit sample of tissue. The extracellular space of tissue is approximately 15% (21), so its void ratio is approximately 0.18.

The concavity C of the ventricular wall can be computed from the following formula, modified from the report by Boas (6),

$$C(x) = \log_{10}\left|\frac{\dfrac{df}{dx}}{\left[1+\left(\dfrac{d^2f}{dx^2}\right)^2\right]^{3/2}}\right| \tag{3}$$

where $f = f(x)$ is a function representing the shape of the ventricular wall. To obtain this analytical curve, the set of points representing the wall are interpolated using a set of Bezier splines (29). Note that the curvature is a function of the position and that we have taken the logarithm to facilitate plotting.

The stretch L of the ventricular wall was computed from

$$L = \frac{dR}{dr} \tag{4}$$

representing the ratio between the original length (dr) of a segment of the ependyma and the new length (dR) after ventricular expansion.

Assessment of accuracy

The finite-element method, like any other numerical analysis technique, is an approximate procedure (41). It is therefore essential to establish the accuracy of the calculations to assess the limits within which the results are meaningful. A number of techniques have been reported for this purpose (8, 10, 57). In this study, a residual (R) analysis (to study the accuracy) and an h-refinement (to study the convergence of the solution) are used.

The residual, sometimes called the force residual, is the difference between the total external forces (F) applied to the domain and the internal reaction forces (I) that arise from the deformed structure (12).

$$R = F - I \tag{5}$$

The smaller the residual, the better the equilibrium between the modeled structure and the real structure and thus the smaller approximation error. However, small residuals are necessary but not sufficient conditions for accuracy; an investigation of the convergence of successive approximations is also required. Here the technique known as h-refinement analysis has been used, which consists of solving the same problem using an increasing number of elements (and thus a smaller size per element). The term h refers to the typical size

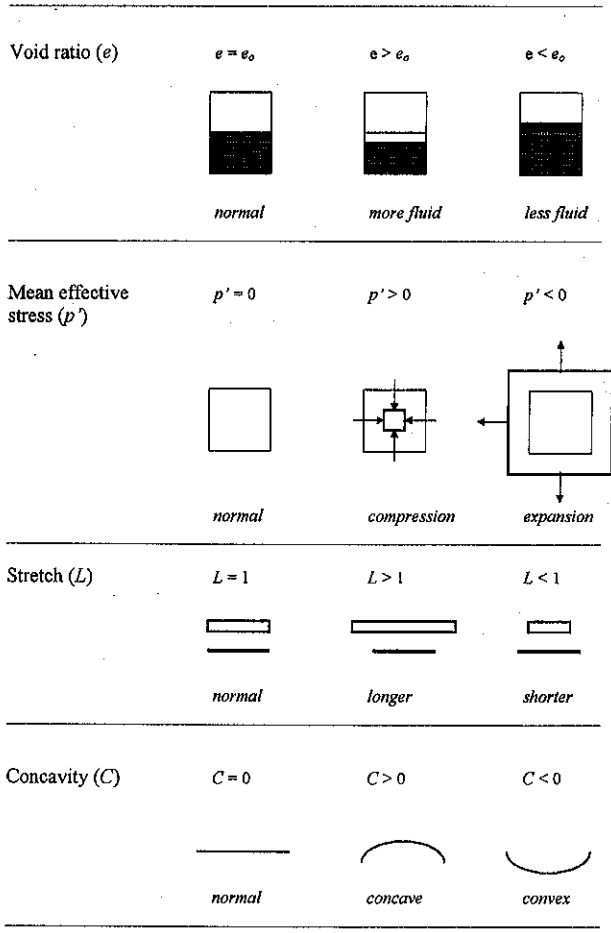

FIGURE 2. Explanatory diagrams for the geometric and mechanical definitions proposed. The void ratio (e) is a measure of the proportion of solids and fluids in a region of tissue. If e_o is the void ratio of the normal brain, then $e > e_o$ corresponds to an increase in fluid content, whereas $e < e_o$ corresponds to a decrease in fluid content. The mean effective stress (p') represents the average solid stress applied to an infinitesimal cube of parenchyma. If the reference state is unpressurized, then $p' = 0$. With $p' > 0$ the reference configuration tends to compress, whereas with $p' < 0$ the configuration tends to expand. The stretch (L) is a measure of the strain along the ventricular wall. If the reference configuration is $L = 1$, then a local elongation of the ventricular wall is characterized by $L > 1$, whereas shortening is described by $L < 1$. The concavity (C) is a measure of the curvature of the ventricular wall with respect to the inside of the ventricles. Therefore, $C > 0$ corresponds to a concave ventricular surface, whereas $C < 0$ corresponds to a convex ventricular surface.

of the elements involved. Because we know that the finite-element approximation has an order of convergence $O(h^3)$ for quadratic elements, a convergent sequence of solutions should indicate the convergence of the numerical solution towards the exact analytical solution.

RESULTS

The results of the finite-element simulation showed the typical progression of hydrocephalus, including ventricular dilation and the appearance of PVL. A progressive expansion of the ventricles was observed (*Fig. 3*). Maximal ventricular distension occurred at $t = 8$ hours, which corresponded to a ventricular pressure of 3 kPa. The outward movement or displacement of the ventricular wall associated with this distension was heterogeneous. At equilibrium, a displacement of almost 7.8 mm was observed for a node at the frontal horn, whereas a node at the thalamus moved only 4.2 mm. This differential displacement resulted in a change in shape from the original ventricular configuration. The horns became "inflated" at the time that the thalamus was effectively displaced and flattened in the radial direction.

Stress concentrations, which were characterized by the mean effective stress p', were also heterogeneous (*Fig. 4*). Areas of compression ($p' > 0$) and expansion ($p' < 0$) were observed. Expansive (tensile) regions where p' varied from -1100 to -360 Pa were found surrounding the anterior and posterior horns. In contrast, compressive regions with p' between +30 and +300 Pa were found near the thalamus and areas with p' between +700 and +1100 Pa were found in the rest of the brain.

Changes in the distribution of the free water of tissue (edema) can be computed from changes in the void ratio. Qualitatively, the graph for the void ratio was almost identical to that for the mean effective stress p', because strain changes are a direct consequence of the applied stress. Because we know that under normal conditions $e_o = 0.18$, an increase in free tissue water (edema) is represented by $e > e_o$ and a decrease by $e < e_o$. Regions in which e was increased were seen surrounding the ventricular horns, where e varied from +0.34 to +0.46. Moving from the ventricles toward the cortex, the void ratio ranged between +0.22 and +0.1 (*Fig. 5*).

The stretch of the ependyma at equilibrium is presented in *Figure 6b*. For most of the domain, the stretch L remained consistently between 0.8 and 1.0, indicating little or no change in length. The exceptions were two peaks of approximately 1.6 and 1.4 that occurred in the regions of the ventricular horns. These values of $L > 1$ indicate that the intercellular spaces of the ependyma are expanding or tearing, so that CSF may pass more freely into the periventricular tissue.

Figure 6a shows the initial concavity (computed from Eq. 3) of the ventricular wall at equilibrium. Two peaks of approximately $C = 12$ units were observed in the regions corresponding to the anterior and posterior ventricular horns. The rest of the domain exhibited a smaller curvature, with C remaining between 8 and 4 units.

To assess the accuracy and convergence of the results, the residual R was computed for each time step of the solution procedure for a sequence of three finite-element meshes, with 679, 1273, and 2421 elements. As theoretically expected, an increase in the number of elements resulted in a decrease of the residual (error) of the approximation. In all cases, how-

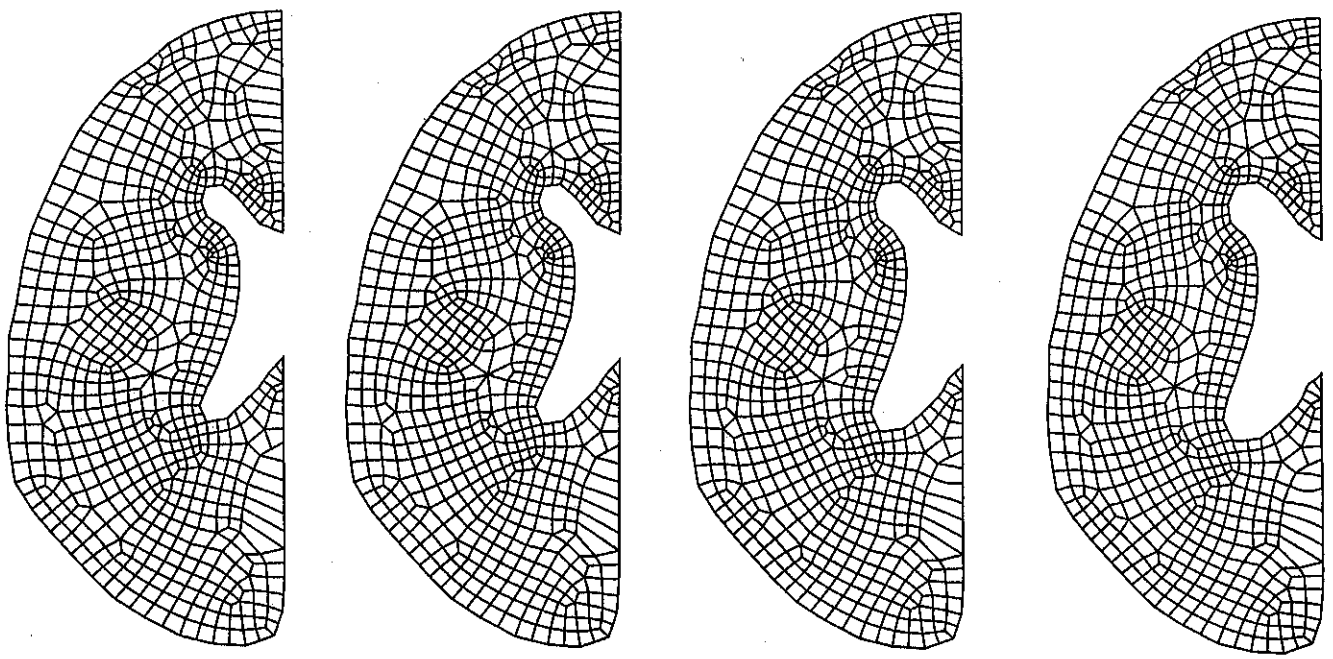

FIGURE 3. Sequence showing ventricular expansion on the finite-element mesh as a result of increased intraventricular pressure at 1, 2, 4, and 8 hours (from *left* to *right*).

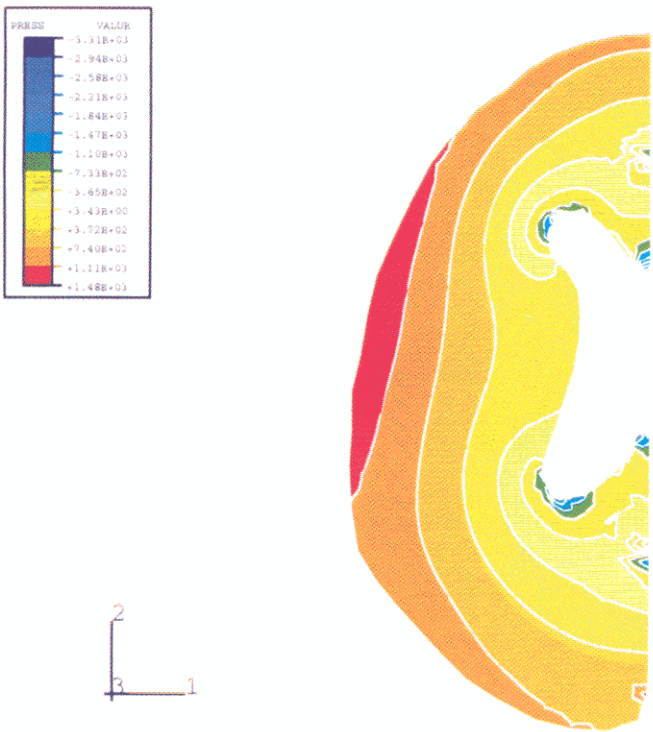

FIGURE 4. Mean effective stress (p') on the tissue after ventricular expansion. The levels of stress range from −3300 Pa (*blue*) to +1480 Pa (*red*). Note the region of expansive stresses ($p' < 0$) surrounding the anterior and posterior horns (*green*) and the region of compressive stresses ($p' > 0$) in the body of the ventricle (*orange*).

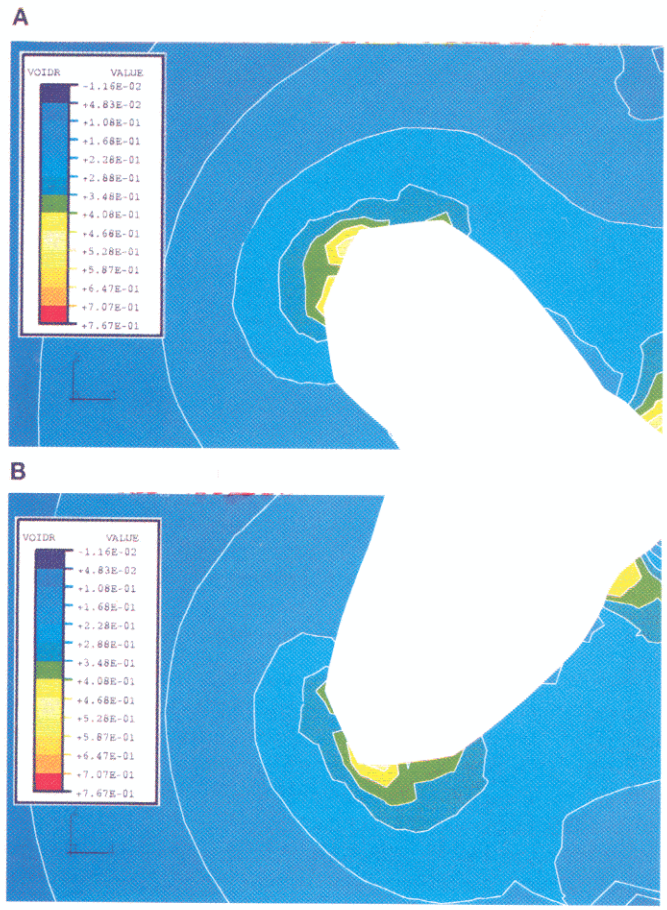

FIGURE 5. Changes in tissue water after ventricular expansion, characterized by changes in its void ratio (e), in the anterior (*A*) and posterior (*B*) ventricular horns. The values for e range from 0 (*blue*) to 0.767 (*red*). Note that the tissue surrounding the anterior horn has an increased water content, i.e., $e = 0.34$ (*green*), which is greater than the normal water content of $e_o = 0.18$. Similarly, the region surrounding the posterior horn has an increased water content of $e = 0.28$ (*green*).

ever, R remained consistently below 5%, suggesting that an acceptable level of accuracy was attained throughout the three simulations.

DISCUSSION

A number of studies have emphasized the importance of biomechanics (17, 18) in the early development of PVL. Our finite-element simulation has allowed the quantitative evaluation of three biomechanical factors, i.e., stress concentrations, disruption of the ependyma, and ventricular geometry, which have been integrated into an explanatory sequence of events that are thought to lead to PVL.

Stress concentrations

Nagashima et al. (42) stated that "ventricular configuration is an important factor in hydrocephalus" and that PVL is attributable to periventricular "stress concentrations, especially at the anterolateral angle of the frontal horn." It is of theoretical and practical importance to determine explicitly to which type of stress these concentrations are referring. In a biphasic material there are three types of stress, i.e., the total stress σ, the effective stress σ', and the pore fluid pressure p. They all produce different effects on the material to which they are applied. Moreover, mathematically the variable stress is a tensorial quantity. A cartesian tensor in three dimensions has nine components and, in the case of stress, six independent ones. The common practice in mechanics is to introduce the mathematical concept of invariants, which are transformations to the stress tensor that obtain some measures of it that are unchanged with coordinate transformations. Some of these invariants fortunately have a physical meaning, which permit us to visualize the deformation behavior of a material. (For an extensive discussion, see, for example, the report by Fung [19]). This is the reason for our choice of p' as a measure of the stress concentrations in the brain parenchyma.

In the simulation, expansive stress concentrations ($p' < 0$) were observed around the ventricular horns and compressive stresses ($p' > 0$) were observed elsewhere (*Fig. 4*). Because stress is linearly related to strain in an elastic material, expansive stresses have the effect of increasing the extracellular spaces of tissue and thus its free water content (in other words, creating PVL). Compressive stresses, in contrast, have the effect of reduc-

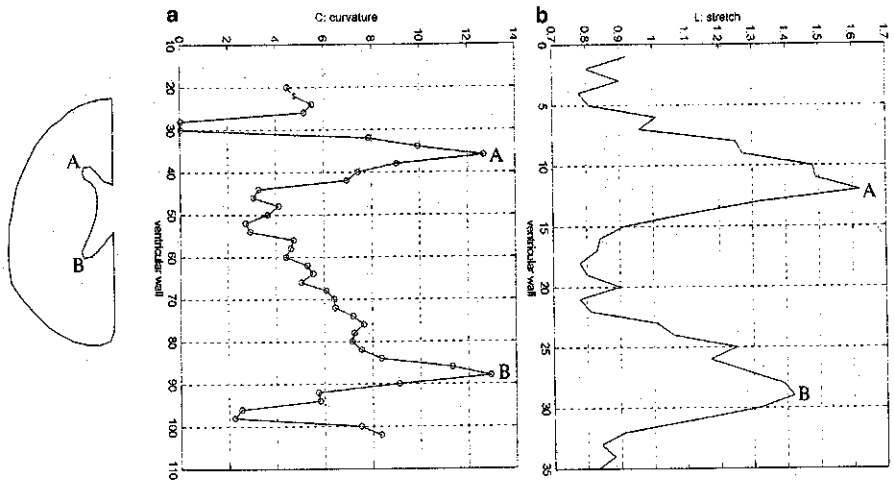

FIGURE 6. Geometric information regarding the ventricular wall, in the form of its curvature before ventricular distension (*a*) and its stretch after ventricular expansion (*b*). The *vertical axes* represent a spatial dimension along the ventricular wall. Points *A* and *B* correspond to the locations of the ventricular anterior and posterior horns, respectively.

ing the extracellular spaces and thus "squeezing out" the free water of tissue (*Fig. 5*). This behavior corresponds to the clinical observations of PVL during the acute stages of hydrocephalus.

Ventricular/subarachnoid pressure gradients

Our model confirms that, for ventricular expansion to occur, a pressure gradient between the ventricle and the subarachnoid space must develop. Such a gradient has been documented experimentally in the acute stages of hydrocephalus (11), but there is debate regarding whether such a gradient persists in the chronic stages.

According to Hooke's law (Eq. A5), the degree of ventricular expansion is a function not only of the gradient but also, and more precisely, of the ratio of this gradient to the stiffness modulus of the tissue. This suggests that a particular gradient could create a substantial ventricular dilation, given that the modulus of the parenchyma is small. In this study, we have chosen a ratio of 0.33 (i.e., 3 kPa/10 kPa), whereas other studies have used values of 0.916 (i.e., 1.1 kPa/1.2 kPa) (51) or 0.27 (i.e., 2.7 kPa/10 kPa) (31).

Conner et al. (11), in cats, experimentally measured a gradient of 5 cm H_2O (0.5 kPa) 7 days after cisternal kaolin injection. Although in absolute terms this is smaller than the gradient of 3 kPa that we used in our simulations, the same gradient/stiffness ratio can be obtained by simply assigning a value of 1.66 kPa to the stiffness modulus of tissue. We computed the resultant ventricular distension with these parameters and found that almost exactly the same deformation patterns as those theoretically expected for a linear elastic material were obtained. For instance, the body of the ventricle had a maximal displacement of 7.47 mm with these parameters, compared with 7.62 mm with the previous ones. Only simultaneous precise measurements of all of these parameters (pressure gradient, ventricular distension, and tissue stiffness) would clarify this issue.

Ventricular geometry

Nagashima et al. (43) stated that "ventricular configuration is an important factor in hydrocephalus." Subramaniam et al. (51), in addition, proposed that "the greater fluid content [PVL] around those regions [the horns] is a function of the curvature of the boundary [the ventricular wall]." In this report we have followed their hypotheses but we have modified the concept of curvature to that of concavity, because curvature by itself yields insufficient information regarding the propensity of tissue to develop edema. *Figure 6a* shows that the regions of maximal concavity of the ventricular wall correspond precisely to the anterior and posterior horns. Moreover, a simple study of the ventricular shape, in relation to the forces produced on the ependyma by the increased intraventricular pressure, is edifying. The concave ventricular wall around the horns suggests that it serves to focus these forces (perpendicular to the ependymal surface) in diverging directions, producing the effect of an effective expansive stress on that region of tissue. In contrast, the convex ventricular wall regions around the thalamus focus the forces in converging directions, producing the effect of an effective compressive stress on that region of tissue (*Fig. 7*). The net effect of these two phenomena is the appearance of edema predominantly around the ventricular horns.

Disruption of ependyma

It is known that during the acute stages of hydrocephalus the ependyma may be stretched and flattened and, in more severe cases, tears may appear (55). Naidich et al. (44) suggested that PVL may be attributable to the intrusion of CSF into the periventricular white matter as a result of mechanical disruption of the ependyma. Our finite-element simulation is based on a linear elastic model for brain tissue. This means that this model does not allow for tears or ruptures appearing in the brain tissue when it is stretched; such a simulation would require an elastoplastic model (33). At this time, the material properties of brain tissue are incompletely defined, and as a first approximation most studies have used either elastic, hyperelastic, or poroelastic models. However, we can begin to study the stretch of the ependyma by measuring how much the elements along the ventricular wall stretch or compress (separate or come together) as the ventricles grow. Our results indicate that the stretch of the ventricular wall closely follows the distribution of PVL (*Fig. 6b*), presenting regions of stretch ($L > 1$) around the horns and areas of compression

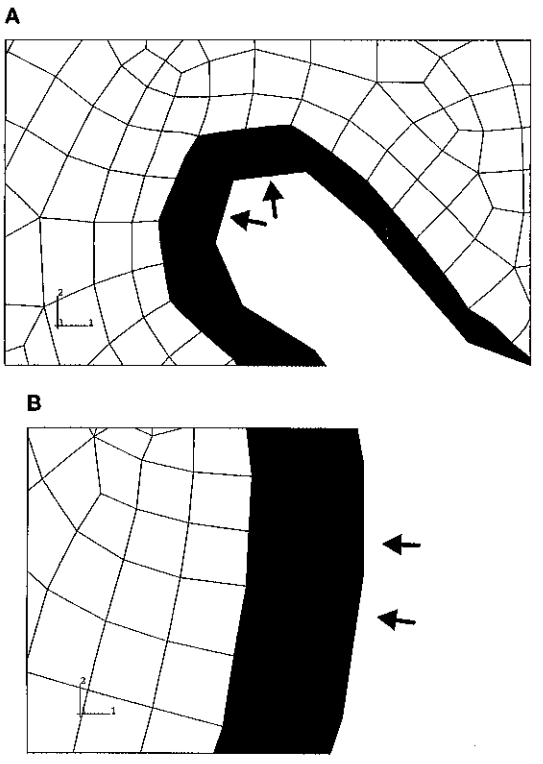

FIGURE 7. Magnified view of the frontal horn (*A*) and the body (*B*) of the ventricle. The *arrows* indicate the orientation of the forces on the ventricular wall generated by the increased intraventricular pressure. The original finite-element mesh, i.e., before deformation, is shown in *gray*, whereas the deformed mesh after ventricular expansion is shown in *white*.

($L < 1$) around the thalamus. So, although we cannot define when rupture occurs in this model, we can state that there is a tendency for the ependymal cells to separate at the horns of the ventricles.

Proposed sequence of events

Although the sequence of events that lead to the appearance of PVL have been known for decades (49), our analysis suggests a rationale for these observed events. In particular, our simulation is a contribution toward understanding the biomechanics of the complex interactions between intraventricular forces and the deformation of the cerebral mantle. A biomechanical sequence of events, incorporating theoretical considerations and the well-known clinical and experimental observations, may be outlined as follows. 1) There is a sudden obstruction to the normal flow of CSF. 2) Because CSF is being continually produced by the choroid plexus, there is a gradual increase in the ventricular fluid pressure. 3) The ventricles expand in proportion to this increased pressure. 4) The resulting compression of the parenchyma produces periventricular stress concentrations but, because of the convex/concave geometry of the ventricular wall, some regions receive expansive stresses (around the horns), whereas others receive compressive stresses (around the thalamus). 5) These expansive stress concentrations around the horns produce a local increase in the extracellular spaces of the tissue and thus initiate the development of interstitial edema. 6) These expansive (tensile) stresses also produce a stretch of the ventricular wall and possibly initiate the rupture and/or opening of the cell junctions of the ependyma, facilitating the development of PVL.

Limitations and future work

The results have a number of limitations. We have assumed constant material properties for the parenchyma. For purely anatomic reasons we can easily imagine that this would not be the case, because tissue would have different stiffnesses when compressed from different directions (anisotropy). More detailed information regarding the elastic and permeability parameters of tissue is required. We are using a two-dimensional approximation of a three-dimensional object. Information regarding the stresses and strains that occur out of the considered plane is lost. The effects of the cerebrovascular system are not considered in this model. A number of studies have also suggested that the observed distributions of PVL are attributable to altered interstitial fluid flow to the ventricle (44). This hypothesis has not been explored in this work. Finally, changes in local metabolic homeostasis are not considered, which means that the results from this study are valid only in a time frame that includes the early stages of the development of hydrocephalus. Clearly, in the future, it will be essential to integrate continuum mechanics for the tissues with the CSF and blood flow dynamics for the craniospinal system (35).

CONCLUSION

Our results seem to corroborate the hypothesis that PVL is a result of both periventricular stress concentrations (in the form of expansive mean effective stresses) and disruption of the ependyma (in the form of stretching of the ependymal cells). The tendency of these forces to appear around the ventricular horns seems to be a direct consequence of the geometry (in the form of the concavity) of the ventricular wall.

ACKNOWLEDGMENTS

We express our gratitude to the following persons and organizations: Dr. Arul Britto and Dr. Ganesh Dasari for expert advice on the use of ABAQUS, Derek Styles (FEMSYS, Ltd.) for kind assistance with the use of FEMGV, especially with the application of the automatic mesh generator, and Dr. Marek Czosnyka, Stefan Piechnik, Dr. Peter Smielewski, Dr. Hugh Richards, Dr. Ashraf El Hammalawi (Eidgenossische Technische Hochschule, Zürich, Switzerland), Dr. Eric A. Schmidt (Department of Neurosurgery, University Hospital, Clermont-Ferrand, France), Dr. Keith A. Johnson (Harvard University), and Dr. J. Alex Becker (Massachusetts Institute of Technology).

Received, September 18, 1998.
Accepted, February 26, 1999.
Reprint requests: John D. Pickard, M.Chir., Academic Neurosurgery Unit, Box 167, Addenbrooke's Hospital, Cambridge CB2 2QQ, England.

APPENDIX A

The linear version of the poroelastic theory is based on the following principles (4):

$$\sigma_{ij} = \sigma'_{ij} - p\delta_{ij} \tag{A1}$$

$$\frac{\partial \sigma_{ij}}{\partial x_j} = 0 \tag{A2}$$

$$\frac{\partial w_j}{\partial t} + K_{ij}\frac{\partial p}{\partial x_i} = 0 \tag{A3}$$

$$e_{ij} = \frac{1}{2}\left[\frac{\partial u_i}{\partial x_j} + \frac{\partial u_j}{\partial x_i}\right] \tag{A4}$$

$$\sigma'_{ij} = \lambda e_{\alpha\alpha}\delta_{ij} + 2\mu e_{ij} \tag{A5}$$

$$\frac{\partial}{\partial t}\frac{\partial w_i}{\partial x_i} + \frac{\partial e}{\partial t} = 0 \tag{A6}$$

$$w_j = n(u_j^f - u_j^s)$$

For the definitions of the variables used, see *Table A1*. Note that the Einstein summation convention is used throughout. The field variables of our model are u_i (a vector quantity), the displacement of the solid phase, and p (a scalar quantity), the pore pressure of the fluid phase of the tissue. Combining Equations A1 through A6, we obtain the field equations for our problem:

$$\mu\frac{\partial^2 u_i}{\partial x_j \partial x_j} + (\mu + \lambda)\frac{\partial e}{\partial x_i} - \frac{\partial p}{\partial x_i} = 0 \tag{A7}$$

$$K_{ij}\frac{\partial^2 p}{\partial x_j \partial x_j} - \frac{\partial e}{\partial t} = 0 \tag{A8}$$

These equations are known as Biot's equations and correspond to a set of elasticity (Eq. A7) and diffusion (Eq. A8) equations with a pressure-coupling term. Our computer simulation is based on the extension of these equations to the finite strain case. This is because only a finite-strain formulation can provide an accurate description of large deformations in a material, such as those encountered in the late stages of obstructive hydrocephalus. The full mathematical development, which is quite involved, can be found, for example, in the report by Coussy (13).

TABLE A1. Definitions of Variables

Symbol	Quantity	Units
σ_{ij}	Total stress	Pa
σ'_{ij}	Effective stress	Pa
p	Fluid pressure	Pa
p'	Mean effective stress	Pa
e	Void ratio	
E	Young's modulus	Pa
ν	Poisson's ratio	
μ	Lame's shear modulus[a]	Pa
λ	Lame's elastic modulus[a]	Pa
w_i	Relative fluid velocity	m/s
x_i	Space coordinate	m
K_{ij}	Hydraulic permeability	$m^4N^{-1}s^{-1}$
e_{ij}	Cauchy's strain	
u, u^s	Displacement of the solid phase	m
u^f	Displacement of the fluid phase	m
t	Time	s
δ_{ij}	Kroenecker delta function	

[a] **Lame's elastic constants can be transformed to the more usual E and ν via $\lambda = E\nu/[(1 + \nu)(1 - \nu)]$ and $\mu = E/[2(1 + \nu)]$ (19).**

TABLE A2. Material Properties of Brain Tissue

Authors (Ref. No.)	Parameter	Value	Species
Flexner et al. (15)	E	37.8–43.3 kPa	Dogs
Galford and McElhaney (20)	E	67 kPa	Human subjects
Metz et al. (38)	E	10–35 kPa	Monkeys
Walsh and Schettini (54)	E	28–41 kPa	Dogs
Reulen et al. (48)	K	1.6×10^{-11} $m^4N^{-1}s^{-1}$	Cats
Grieschafer et al. (23)	E	30 kPa	Cattle
Guillaume et al. (24)	E^a	46.8 ± 31.3 kPa	Cattle
Guillaume et al. (24)	E^b	106 ± 73.9 kPa	Cattle
Guillaume et al. (24)	ν	0.32–0.37	Cattle

[a] **Refers to nonperfused brain.**
[b] **Refers to perfused brain.**

APPENDIX B

A linear poroelastic material can be characterized by a set of three parameters, i.e., Young's modulus (E), Poisson's ratio (ν), and hydraulic permeability (K). This set of material parameters must be measured experimentally for brain tissue. A review of the literature has shown the values presented in *Table A2*.

It is interesting to note that the range of E remains consistently between 10 and 100 kPa. It is also interesting to note that the values reported by Guillaume et al. (24) were somewhat out of that range when they were measured in perfused brains. Apparently this is attributable to the fact that the cerebrovascular bed, which occupies approximately 7% of the total brain contents (32) and has a more or less homogeneous distribution, contributes to the stiffness of the brain. Measurements for the permeability have been very scant. Reulen et al. (48) obtained a value of $K = 1.6 \times 10^{-11}$ $m^4N^{-1}s^{-1}$ by measuring the spread of sodium fluorescin dye through the parenchyma in cold infused edema. For an excellent discussion of the significance of material parameters for poroelastic analyses, see the report by Kaczmarek et al. (31).

REFERENCES

1. Adams JH, Graham DI: *An Introduction to Neuropathology*. New York, Churchill-Livingstone, 1994.
2. Alp MS: Periventricular lucency on computed tomography associated with hydrocephalus: What is the cause? **Surg Neurol** 44: 285–286, 1995.
3. Asada M, Tamaki N, Kanazawa Y, Matsumoto S, Matsuo M, Kimira S, Fujii S, Kaneda Y: Computer analysis of periventricular lucency on the CT scan. **Neuroradiology** 16:207–211, 1978.
4. Biot MA: General theory of three dimensional consolidation. **J Appl Phys** 12:1244–1258, 1941.
5. Biot MA: Mechanics of deformation and acoustic propagation in porous media. **J Appl Phys** 33:1482–1498, 1962.
6. Boas ML: *Mathematical Methods in the Physical Sciences*. New York, Wiley, 1983.
7. Bowen RM: Incompressible porous media models by the theory of mixtures. **Int J Engl Sci** 18:1129–1148, 1980.
8. Braess D: *Finite Elements: Theory, Fast Solvers, and Applications in Solid Mechanics*. New York, Cambridge University Press, 1997.
9. Braun KP, Dijkhuizen RM, de Graaf RA, Nicolay K, Vandertop WP, Gooskens RH, Tulleken KA: Cerebral ischemia and white matter edema in experimental hydrocephalus: A combined in vivo MRI and MRS study. **Brain Res** 757:295–298, 1997.
10. Burnett DS: *Finite Element Analysis: From Concepts to Applications*. Reading, Addison-Wesley, 1987.
11. Conner ES, Foley L, Black PM: Experimental normal-pressure hydrocephalus is accompanied by increased transmantle pressure. **J Neurosurg** 61:322–327, 1984.
12. Cook RD, Malkus DS, Plesha ME: *Concepts and Applications of Finite Element Analysis*. New York, Wiley, 1984.
13. Coussy O: *The Mechanics of Porous Continua*. New York, Wiley, 1995.
14. FEMSYS, Ltd.: *FEMGV5*. Leicester, UK, FEMSYS, Ltd., 1998.
15. Flexner LB, Clark JH, Weed LW: The elasticity of the dural sac and its contents. **Am J Physiol** 101:293–303, 1932.
16. Fung YC: *Foundations of Solid Mechanics*. Englewood Cliffs, Prentice-Hall, 1964.
17. Fung YC: *Biomechanics: Motion, Flow, Stress and Growth*. New York, Springer-Verlag, 1990.
18. Fung YC: *Biomechanics: Mechanical Properties of Living Tissues*. New York, Springer-Verlag, 1991.
19. Fung YC: *A First Course in Continuum Mechanics*. Englewood Cliffs, NJ, Prentice-Hall, 1994.
20. Galford JE, McElhaney JH: A viscoelastic study of scalp, brain and dura. **J Biomech** 3:211–221, 1970.
21. Geschwind N: The mechanism of normal pressure hydrocephalus. **J Neurol Sci** 7:481–493, 1968.
22. Gopinath G, Bhatia R, Gopinath PG: Ultrastructural observations in experimental hydrocephalus in the rabbit. **J Neurol Sci** 43:333–344, 1979.
23. Grieschafer F, Lewek J, Faust U, Nagel JH: FEM as a tool for minimally invasive brain surgery. National Association for the Finite Element Method, World Congress Proceedings, 1997, pp 728–737.
24. Guillaume A, Osmont D, Gaffe D, Sarron JC, Wuandieu P: Effects of perfusion on the mechanical behaviour of the brain exposed to hypergravity. **J Biomech** 30:383–389, 1997.
25. Hakim S: Biomechanics of hydrocephalus. **Acta Neurol Latinoam** 17[Suppl 1]:169–194, 1971.
26. Hakim S, Venegas JG, Burton JD: The physics of the cranial cavity, hydrocephalus and normal pressure hydrocephalus: Mechanical interpretation and mathematical model. **Surg Neurol** 5:187–210, 1976.
27. Higashi K, Noda Y, Tachibana S: Study of brain tissue impedance in the hydrocephalic cat. **J Neurol Neurosurg Psychiatry** 52:636–642, 1989.
28. Hilbitt, Karlsson, Sorensen, Inc.: *ABAQUS/Standard User's Manual, Version 5.7*. Pawtucket, RI, HKS Publishing, 1998.
29. Iserles A: *A First Course in the Numerical Analysis of Differential Equations*. New York, Cambridge University Press, 1997.
30. Johnson KA, Becker JA: The Whole Brain Atlas. Available at http://www.med.harvard.edu:80/AANLIB/home.html.
31. Kaczmarek M, Subramaniam RP, Neff SR: The hydromechanics of hydrocephalus: Steady-state solutions for cylindrical geometry. **Bull Math Biol** 59:295–323, 1997.
32. Kaye AH: *Essential Neurosurgery*. New York, Churchill-Livingstone, 1997, ed 2.
33. Lubliner J: *Plasticity Theory*. New York, Macmillan, 1990.
34. Mandel J: Consolidation des sols (etude mathematique). **Geotechnique** 3:287–299, 1953.
35. Marmarou A, Maset A, Ward JD, Choi S, Young SF: Contribution of CSF and vascular factors to evolution of ICP in severely head injured patients. **J Neurosurg** 66:883–890, 1987.
36. Marmarou A, Shulman K, Rosende R: A nonlinear analysis of the cerebrospinal fluid system and intracranial pressure dynamics. **J Neurosurg** 48:332–344, 1978.
37. Matsumae M, Kikinis R, Morocz I, Lorenzo AV, Albert MS, Black PM, Jolesz FA: Intracranial compartment volumes in patients with enlarged ventricles assessed by magnetic resonance-based image processing. **J Neurosurg** 84:972–981, 1996.
38. Metz H, McElhaney J, Ommaya AK: A comparison of the elasticity of live, dead, and fixed brain tissue. **J Biomech** 3:453–458, 1970.
39. Moseley IF, Radii EW: Factors influencing the development of periventricular lucencies in patients with raised intracranial pressure. **Neuroradiology** 17:65–69, 1979.
40. Murata T, Handa H, Mori K, Nakano Y: The significance of periventricular lucency on computed tomography: Experimental study with canine hydrocephalus. **Neuroradiology** 20:221–227, 1981.
41. NAFEMS: *Guidelines to Finite Element Practice, National Association for the Finite Element Method*. Glasgow, Bell and Bain Publishers, 1992.
42. Nagashima T, Tamaki N, Matsumoto S, Horwitz B, Seguchi Y: Biomechanics of hydrocephalus: A new theoretical model. **Neurosurgery** 21:898–904, 1987.
43. Nagashima T, Tamaki N, Matsumoto S, Seguchi Y: Biomechanics and a theoretical model for hydrocephalus: Application of the finite-element method, in Miller JD, Teasdale GM, Rowan JO, Galbraith SL, Mendelow AD (eds): *Intracranial Pressure VI*. New York, Springer-Verlag, 1986, pp 441–446.
44. Naidich TP, Epstein F, Lin JP, Kricheff II, Hochwald GM: Evaluation of paediatric hydrocephalus by computed tomography. **Radiology** 11:337–345, 1976.
45. Nakano H, Bandoh K, Miyaoka M, Sato K: Evaluation of hydrocephalic periventricular radiolucency by dynamic computed tomography and xenon-computed tomography. **Neurosurgery** 39: 758–762, 1996.
46. Nyberg-Hansen R, Torvik A, Bhatia R: On the pathology of experimental hydrocephalus. **Brain Res** 95:343–350, 1975.
47. Peña A: A theoretical study of brain biomechanics via poroelastic theory and the finite element method. Cambridge, UK, University of Cambridge, 1996 (dissertation).
48. Reulen HJ, Graham R, Spatz M, Klatzo I: Role of pressure gradients and bulk flow in dynamics of vasogenic brain edema. **J Neurosurg** 46:24–35, 1977.

nounced in areas of severe ependymal damage, there is edema of the white matter (5, 8). This is the earliest pathological finding involving the brain parenchyma and occurs in specific sites at specific times. At the dorsal angles of the lateral ventricle, for example, the periventricular white matter becomes edematous at 3 to 6 hours. The margin of edema spreads thereafter and reaches the white matter of the centrum semiovale by 19 to 24 hours (5, 6, 8).

When isotopes or tracer dyes are injected into the ventricles of acutely hydrocephalic animals, a significant increase in the ventricular permeability can be demonstrated (1, 6, 8). The increase becomes apparent as soon as the pathological changes in the ependyma become apparent (1–3 h), and the permeability is greatest at points of severe ependymal damage (5, 6, 8). Taken together, these findings indicate that increased intraventricular pressure, acting in concert with the pathological changes in the ventricular wall, results in flow of CSF out of the ventricles at points of least resistance (1, 4–6, 8).

The results of this study confirm and extend pathological findings in acute obstructive hydrocephalus. Evidence that the geometry of the ventricular wall serves to focus the forces associated with increased intraventricular pressure is not surprising. Less well appreciated are counterforces, created by variations in the density of gray and white matter, that influence the formation of PVL.

Thomas H. Milhorat
Brooklyn, New York

1. Levin VA, Milhorat TH, Fenstamacher JD, Hammock MK, Rall DP: Physiological studies on the development of obstructive hydrocephalus in the monkey. **Neurology** 21:238–246, 1971.
2. Milhorat TH: Acute hydrocephalus. **N Engl J Med** 283:857–859, 1970.
3. Milhorat TH: Experimental hydrocephalus: Part I—A technique for producing obstructive hydrocephalus in the monkey. **J Neurosurg** 32:385–389, 1970.
4. Milhorat TH: *Hydrocephalus and the Cerebrospinal Fluid*. Baltimore, Williams & Wilkins, 1972, pp 129–132.
5. Milhorat TH, Clark RG: Experimental hydrocephalus: Part III—Light microscopic findings in acute and subacute obstructive hydrocephalus in the monkey. **J Neurosurg** 32:400–413, 1970.
6. Milhorat TH, Clark RG: Some observations on the circulation of phenolsulfonphthalein in cerebrospinal fluid: Normal flow and the flow in hydrocephalus. **J Neurosurg** 32:522–528, 1970.
7. Milhorat TH, Clark RG, Hammock MK: Experimental hydrocephalus: Part II—Gross pathological findings in acute and subacute obstructive hydrocephalus in the dog and monkey. **J Neurosurg** 32:390–399, 1970.
8. Milhorat TH, Clark RG, Hammock MK, McGrath PP: Structural, ultrastructural, and permeability changes in the ependyma and surrounding brain favoring equilibration in progressive hydrocephalus. **Arch Neurol** 22:397–407, 1970.

The authors used finite-element mechanical models to study the changes in ventricular shape and their effects in the acute stage of the hydrocephalic process, particularly the reason for periventricular lucency concentrated in the horns of the ventricles. Peña et al. provide an elegant description of the biomechanical process leading to ventricular dilation. Of importance is the fact that the results of experimental cat studies with kaolin injections and the theoretical predictions of the model are in excellent agreement. Despite the mathematical complexity, the authors have taken great care to explain these phenomena in the simplest of terms. Their analysis has demonstrated that, with obstruction of CSF outflow, ventricular dilation approaching 2 cm develops in response to a 22.5-mm Hg gradient between the ventricles and the subarachnoid space, in an 8-hour period.

The hypothesis of Hakim et al. (Refs. 25 and 26 in the article), i.e., that the brain acts like a sponge and water squeezed out of the ventricles expands, is supported by the analysis. The study also dispels the notion that periventricular lucency, as seen in magnetic resonance imaging scans, may be artifactual. Although the cerebrovascular system is not represented in this initial work, I look forward to an expansion of the modeling effort and the eventual incorporation of both CSF and vascular elements.

Anthony Marmarou
Richmond, Virginia

The biomechanical forces that lead to ventricular dilation and the development of PVL in communicating hydrocephalus are investigated by computer simulation using bioengineering principles. There are extensive and comprehensive definitions of the effects of ventricular configuration, brain tissue properties, and transventricular forces on these processes. The authors have carefully presented the basic assumptions of their proposed biological system and the limitations of their methods. The computer simulation accurately predicted that the greatest dilation of the ventricular system would be at the anterior and posterior horns, the site of greatest PVL, because of the concave configuration of the ventricular horns and the effective tissue pressure gradient. The authors also demonstrated the greatest lengthening of the ependymal wall at this site. Presumably the changes in the ventricular wall (changes in the cell junctions or actual rupture) increase the permeability of this barrier and increase the movement of ventricular fluid down a pressure gradient, leading to the development of PVL. As carefully pointed out by the authors, the effects of the cerebrovascular system, variations in tissue properties, and local changes in metabolic homeostasis are limitations to this study. The latter factor, but perhaps the other limitations as well, make the results valid only for the short time frame investigated in this study. The basic methods seem to have great utility, and further studies should take these limitations into consideration and define the more chronic state and the effects of aging on this process.

Michael Pollay
Sun City West, Arizona

The authors have used a mathematical model of the brain to examine the changes in acute hydrocephalus. Their model supports one theory of the development of PVL, namely the concentration of expansile stress at the frontal and occipital horns, resulting in increased interstitial spaces.

The model is fairly sophisticated and uses a poroelastic matrix, with saturated interstitial fluid, and finite-element analysis to develop a numerical solution. As noted by the authors, this type of analysis has been performed previously. The authors used what is, in our opinion, a more realistic value for the Poisson ratio (1, 4) and focused on the changes in the curvature of the ventricular wall. As they point out, the mechanical parameters of the brain have been infrequently measured and are critical for this type of analysis.

The model uses a rather large pressure gradient across the ventricular wall in a short time period. Although this is an important first step, analysis of the development of chronic hydrocephalus and its response to the insertion of a ventriculoperitoneal shunt would be much more interesting and of much wider applicability. It is unlikely that this particular model, which is linear, could be extrapolated to large changes in ventricular size. Further progress in the management of hydrocephalus is dependent on the development of more sophisticated mathematical models of brain biomechanics. Previous assumptions based on simple compartment models (2, 3) have helped explain the short-term effects of shunts, but the shunt designs have not performed as predicted in the long term. Collaborations between mathematicians and neurosurgeons, as in this report, should be strongly encouraged and could lead to further progress in this fascinating area.

James M. Drake
Toronto, Ontario, Canada

---

1. Drake JM, Mostachfi O, Tenti G, Sivaloganathan S: Realistic simple mathematical model of brain biomechanics for computer simulation of hydrocephalus and other brain abnormalities. **Can J Neurol Sci** 23[Suppl 1]:S33, 1996 (abstr).
2. Drake JM, Tenti G, Sivaloganathan S: Computer modeling of siphoning for CSF shunt design evaluation. **Pediatr Neurosurg** 21:6–15, 1994.
3. Sivaloganathan S, Tenti G, Drake JM: Mathematical pressure-volume models of the cerebrospinal fluid. **Appl Math Comput** 94:243–266, 1998.
4. Tenti G, Sivaloganathan S, Drake JM: Rain biomechanics: Steady-state consolidation theory of hydrocephalus. **Can Appl Math Q** (in press).